4.6. Photophysical and electrochemical investigation

Photophysical and electrochemical investigations were done by Bologna team: Filippo Marchioni, Margherita Venturi, and Vincenzo Balzani at Dipartimento di Chimica "G. Ciamician", Università di Bologna, Italy. Parts of the text used here were already published.

4.6.1. Photophysical properties of macrocycle 103c and its Ru and Os complexes

Photophysical properties of macrocycle 103c

Macrocycle **103c** shows in dichloromethane solution an intense absorption in the UV region (λ_{max} = 314 nm, ε = 109000 $M^{-1}cm^{-1}$) (Figure 83) and a fluorescence band (λ_{max} = 380 nm, τ = 0.7 ns, and Φ = 0.7). In chloroform/dichloromethane 1:1 rigid matrix at 77 K, the emission band is slightly blue shifted (λ_{max} = 378 nm) and the emission lifetime is slightly longer (τ = 0.8 ns).

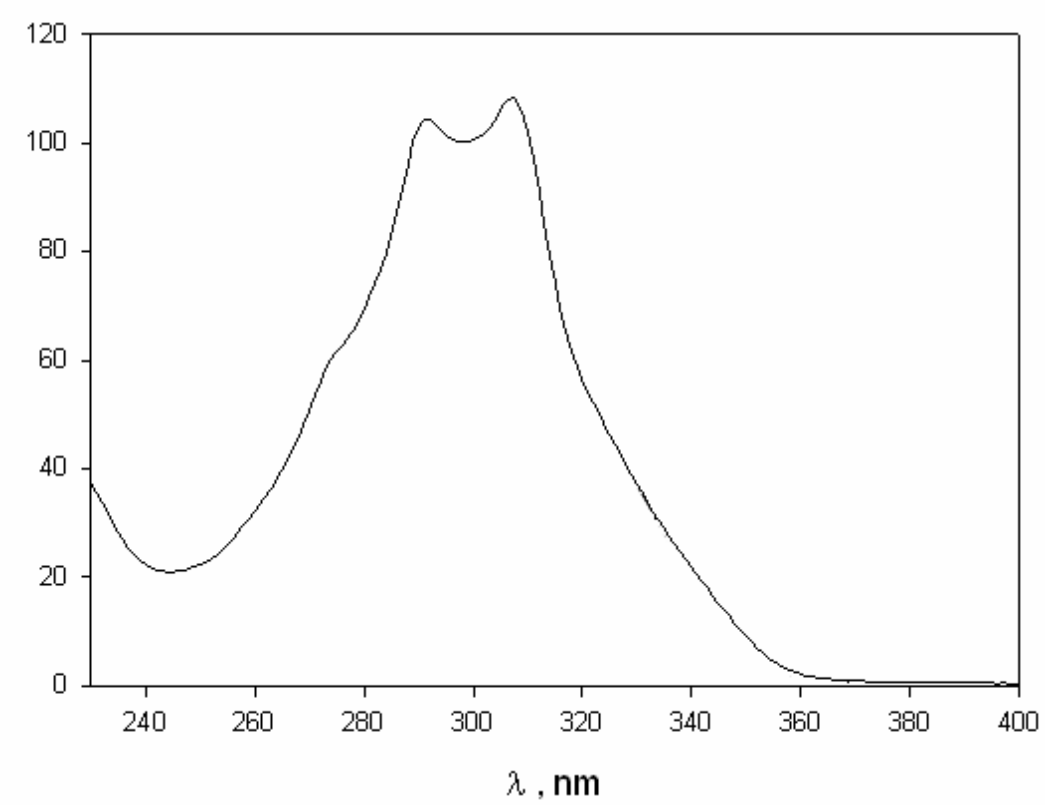

Figure 83. Absorption spectra in dichloromethane solution of macrocyclic ligand **103c**.

Photophysical properties of $[(bpy)_2Ru(103c)](PF_6)_2$

In dichloromethane solution, $[(bpy)_2Ru(\mathbf{103c})]^{2+}$ exhibits an absorption band at λ = 455 nm (ε_{max} = 10400 $M^{-1}cm^{-1}$, Figure 84) and an emission band at λ = 619 nm (τ = 733 ns, Φ = 0.05, Figure 84). These bands can straightforwardly be assigned to spin-allowed and, respectively, spin-forbidden metal-to-ligand-charge-transfer (MLCT) excited states, characteristic of Ru(II) polypyridine complexes[86],[87],[88]

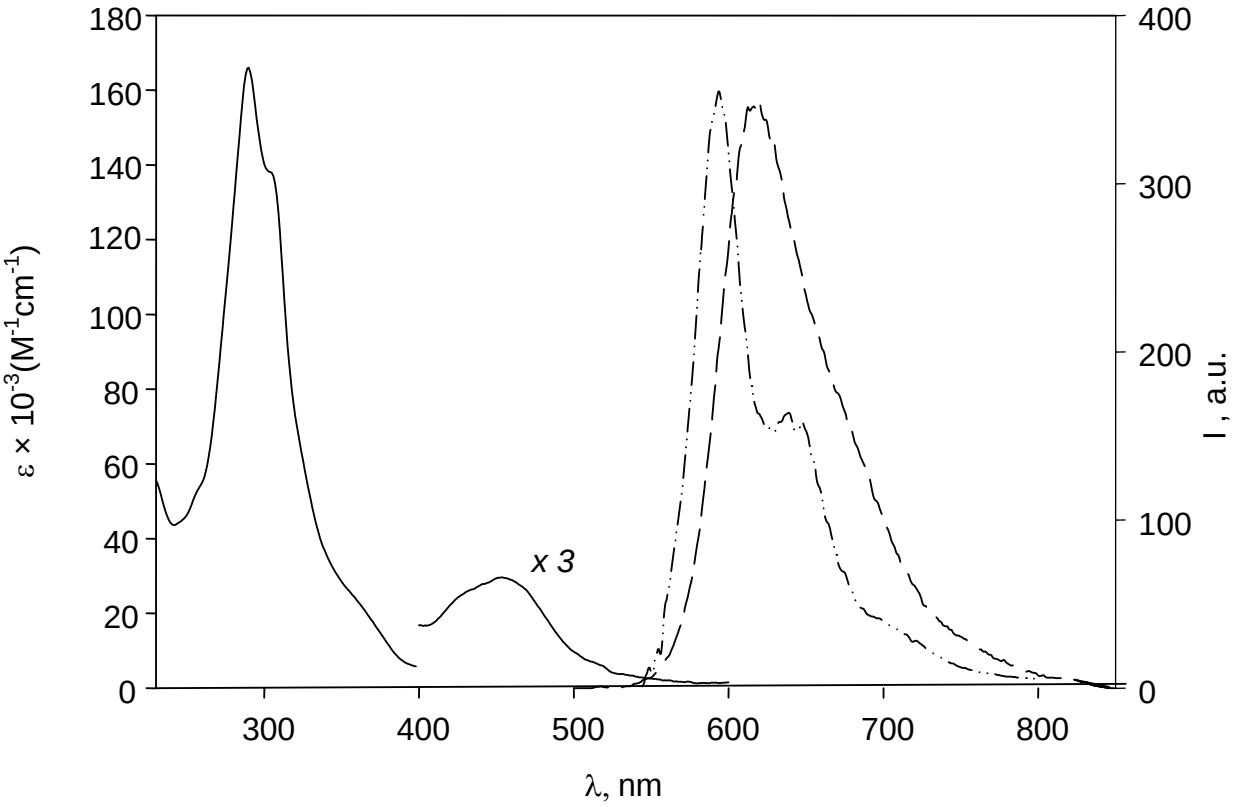

Figure 84. Absorption (dichloromethane solution, full line) and emission (dichloromethane solution at 298 K, dashed line; dichloromethane/methanol rigid matrix at 77 K, dashed and dotted line) spectra of $[(bpy)_2Ru(\mathbf{103c})]^{2+}$.

In a rigid dichloromethane/methanol (1:1 v/v) matrix at 77 K, $[(bpy)_2Ru(\mathbf{103c})]^{2+}$ shows a structured emission band with λ_{max} = 593 nm (Figure 84) and τ = 5.5 μs, again typical of Ru(II) polypyridine complexes[86].

Photophysical properties of $[(bpy)_2Os(103c)](PF_6)_2$

In dichloromethane solution, the $[(bpy)_2Os(\mathbf{103c})]^{2+}$ exhibits absorption (λ_{max}= 490 nm, ε_{max} = 8000 $M^{-1}cm^{-1}$; λ_{max}= 650 nm, ε_{max} = 2000 $M^{-1}cm^{-1}$) and emission bands (λ_{max} = 745 nm, τ = 80 ns, Φ = 0.002) in the visible region. These bands, straightforwardly assigned to spin-allowed and, respectively, spin-forbidden MLCT excited states, are characteristic of the Os(II) polypyridine complexes.[48a]

4.6.2. Electrochemical properties of macrocycle 103c and its Ru and Os complexes

Electrochem properties of macrocycle 103c

The electrochemical properties of macrocyclic ligand **103c** were investigated in purified tetrahydrofuran under vacuum conditions. In the accessible potential window (+1/–3 V vs SCE), compound **103c** undergoes two reversible and monoelectronic reduction processes at –1.78 and –2.02 V *vs* SCE, and no oxidation process (Table 10).

Table 10. Redox potentials [a]

	Ligand centered reduction $E_{1/2}$, V vs SCE		Metal centered oxidation $E_{1/2}$, V vs SCE	
			Os	Ru
103c [b]	–2.02	–1.78		
$[(bpy)_2Ru(\mathbf{103c})]^{2+}$	–1.47	–1.12		+1.45
$[(bpy)_2Os(\mathbf{103c})]^{2+}$	–1.36	–1.03	+1.03	
$[Ru(bpy)_3]^{2+}$	–1.50	–1.24		+1.43
$[Os(bpy)_3]^{2+}$	–1.35	–1.06	+1.03	

[a]Room temperature argon-purged dichloromethane solution and reversible and monoelectronic processes, unless otherwise noted; tetrabutylammonium hexafluorophosphate as supporting electrolyte, glassy carbon as working electrode. [b]Purified tetrahydrofurane under vacuum conditions.

Electrochem properties of $[(bpy)_2Ru(103c)](PF_6)_2$

In the electrochemical experiments performed in argon-purged dichloromethane solution (accessible potential window: +1.7/–1.7 V vs SCE), $[Ru(bpy)_2(\mathbf{103c})]^{2+}$ undergoes a reversible monoelectronic oxidation at +1.45 V *vs* SCE (Table 10), that can be assigned to the oxidation of the metal-center[48a]. The potential value at which the Ru ion is oxidized is similar to that observed for the metal oxidation in the model compound $[Ru(bpy)_3]^{2+}$ (Table 10). On reduction, two reversible and monoelectronic processes are observed in the accessible potential window, which are attributed to the reduction of the ligands (Table 10).[48a] By comparison with the data obtained for $[Ru(bpy)_3]^{2+}$ (Table 10), the first process at –1.12 V *vs* SCE is assigned to the reduction of the bpy unit of the macrocycle **103c**, considering that such a ligand is easier to reduce than bpy, whereas the second process at –1.47 V *vs* SCE involves one of the bpy ligands. This process occurs at a potential value which is (a) more negative than that of the first reduction of $[Ru(bpy)_3]^{2+}$, because in $[(bpy)_2Ru(\mathbf{103c})]^{2+}$ the bpy reduction is preceded by the reduction of the bpy unit of **103c**, and (b) less negative than that of the second reduction of $[Ru(bpy)_3]^{2+}$ because of the greater delocalization of the charges introduced by replacement of one bpy with the ligand **103c**.

Electrochem properties of $[(bpy)_2Os(103c)](PF_6)_2$

In the electrochemical experiments performed in argon-purged dichloromethane solution, $[Os(bpy)_2(\mathbf{103c})]^{2+}$ undergoes a reversible monoelectronic oxidation at +1.03 V *vs* SCE (Figure 85, Table 10), that can be assigned to the oxidation of the Os ion.[48a].

The potential value at which the metal ion is oxidized is very close to those obtained for the metal oxidation in the model compound $[Os(bpy)_3]^{2+}$ (Table 10). On reduction, two reversible and monoelectronic processes are observed in the accessible potential window (Figure 85, Table 10).

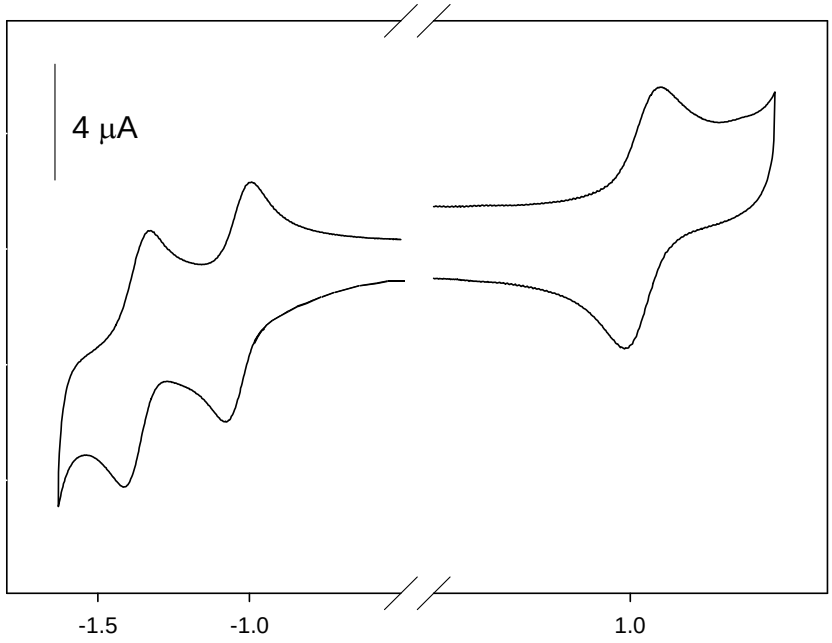

Figure 85. Cyclic voltammogram obtained for $[Os(bpy)_2(\mathbf{103c})]^{2+}$ complex (argon-purged dichloromethane; complex concentration 4×10^{-4} M; glassy carbon as working electrode, scan rate of 100 mV/s).

The first process at –1.03 V *vs* SCE is assigned to the reduction of ligand **103c**, while the second process at –1.36 V *vs* SCE concerns the reduction of one of the two bpy ligands. The fact that in $[Os(bpy)_2(\mathbf{103c})]^{2+}$ these processes occur at potential values very similar to those observed for $[Os(bpy)_3]^{2+}$ can be explained by considering that the Os ion is capable of delocalizing the introduced charges better than the Ru ion.[89]

4.6.3. Photophysical properties of macrocycle 10 and its Ru and Os complexes

Photophysical properties of macrocycle 10

A dichloromethane solution containing 4×10^{-6} M of **10** shows a structured absorption band in the UV region with λ_{max}= 305 nm (ε_{max} = 118000 $M^{-1}cm^{-1}$) (Figure 86, Table 11) and an extremely intense fluorescence band with λ_{max} = 381 nm (Figure 87), τ = 0.8 ns, and Φ = 0.9 (Table 11). Because of the high molar absorption coefficient and the very high fluorescence quantum yield, emission can clearly be seen even for solutions having nanomolar concentration. In a rigid butyronitrile matrix

at 77 K (Table 11), the emission band is slightly blue shifted (λ_{max} = 375 nm) and the emission lifetime is slightly increased (1.0 ns).

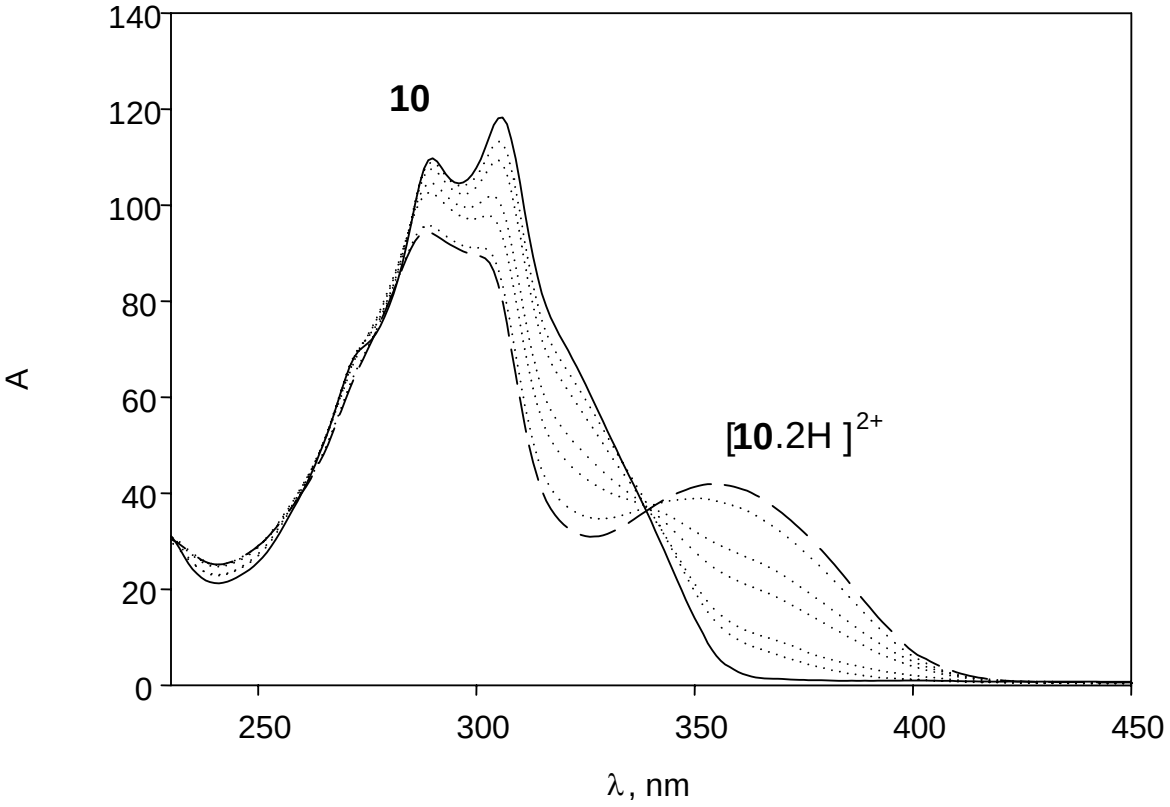

Figure 86. Absorption spectral changes observed during the titration of **10** with trifluoromethanesulfonic acid in dichloromethane solution.

Table 11. Absorption and emission properties

Ligand	Absorption[a]		Luminescence				
	298 K		298 K [a]			77 K	
	λ_{max}, nm	ε ($M^{-1}cm^{-1}$)	λ_{max}, nm	τ, ns	Φ	λ_{max}, nm	τ, ns
10	305	118000	381	0.8	0.9	375[b]	0.001[b]
[**10**.2H]$^{2+}$	355	42000	520				

[a] Dichloromethane solution. [b] Butyronitrile rigid matrix.

When a dichloromethane 4×10^{-6} M solution of **10** was titrated with trifluoromethanesulfonic acid strong spectral changes were observed. A decrease in

the intensity of the 305 nm absorption band was accompanied by the formation of a new band with λ_{max} = 355 nm and ε_{max} = 42000 $M^{-1}cm^{-1}$ (Figure 86, Table 11). In the fluorescence spectrum, the disappearance of the intense band (λ_{max} = 381 nm) is accompanied by the appearance of a broad and weak band with λ_{max} = 520 nm (Figure 87, Table 11). The protonation reaction is fully reversible upon addition of tributylamine.

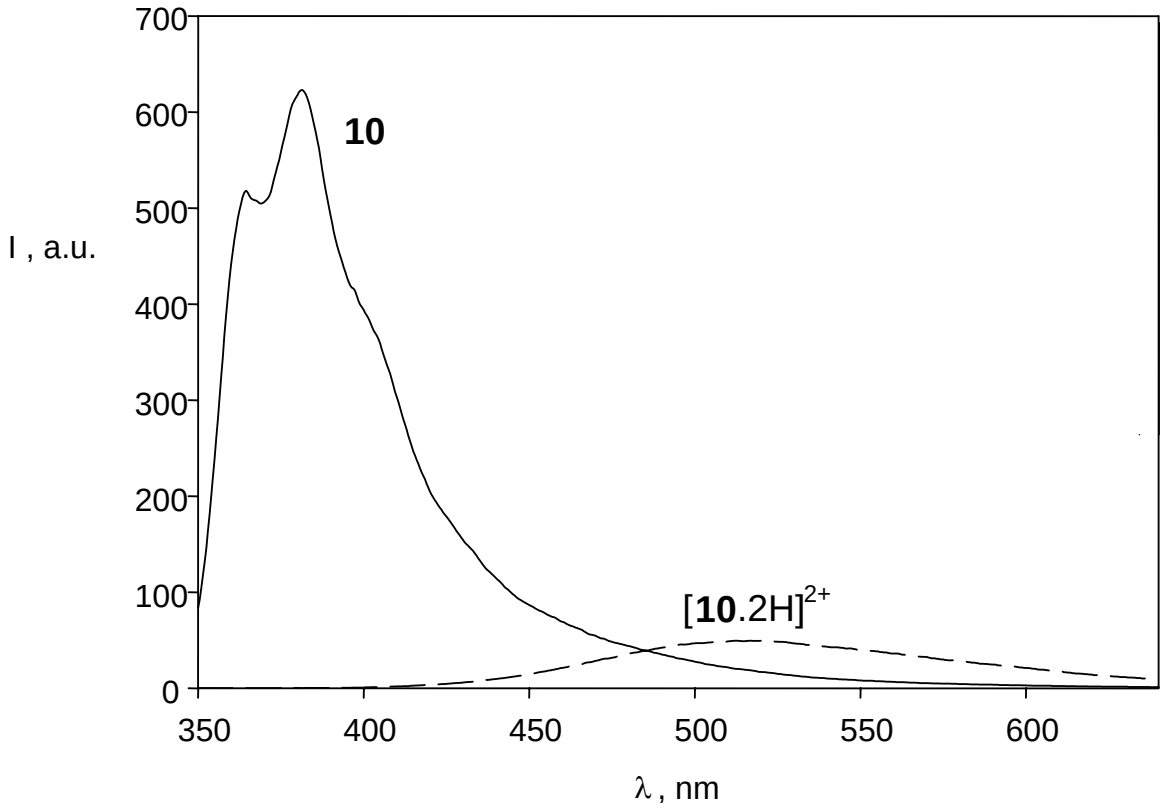

Figure 87. Emission spectra of **10** and [**10.**2H]$^{2+}$ in dichloromethane solution.

Photophysical properties of $[(bpy)_2Ru(10)Ru(bpy)_2](PF_6)_4$

In dichloromethane solution, the $[(bpy)_2Ru(\mathbf{10})Ru(bpy)_2]^{4+}$ complex exhibits absorption (λ_{max} = 453 nm, ε_{max} = 19000 $M^{-1}cm^{-1}$) and emission bands (λ_{max} = 625 nm, τ = 792 ns, Φ = 0.05) in the visible region (Figure 88). These bands can straightforwardly be assigned to spin-allowed and, respectively, spin-forbidden metal-to-ligand-charge-transfer (MLCT) excited states, characteristic of Ru(II) polypyridine complexes.[48a], [86] In a rigid methanol/dichloromethane (1:1 v/v) matrix at 77 K,

$[(bpy)_2Ru(\mathbf{10})Ru(bpy)_2]^{4+}$ shows a structured emission band with λ_{max} = 600 nm (Figure 88) and τ = 5.14 µs, again typical of Ru(II) polypyridine complexes.

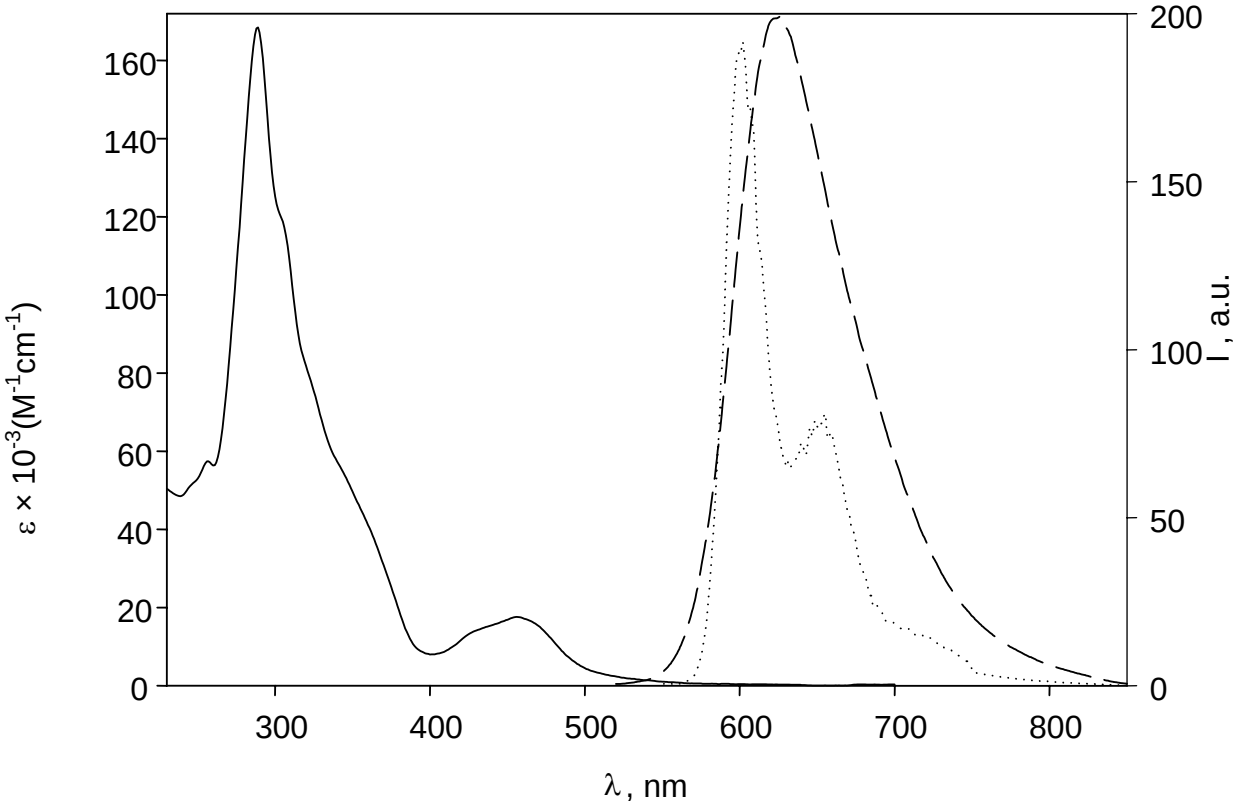

Figure 88. Absorption (dichloromethane solution; full line) and emission (dichloromethane solution at 298 K, dashed line; methanol/dichloromethane rigid matrix at 77 K, dotted line) spectra of the $[(bpy)_2Ru(\mathbf{10})Ru(bpy)_2]^{4+}$ complex.

Photophysical properties $[(bpy)_2Os(10)Os(bpy)_2]^{4+}$

In dichloromethane solution, the $[(bpy)_2Os(\mathbf{10})Os(bpy)_2]^{4+}$ complex exhibits absorption (λ_{max}= 488 nm, ε_{max} = 15500 $M^{-1}cm^{-1}$) and emission bands (λ_{max} = 740 nm, τ = 59 ns, Φ = 0.003) in the visible region (Figure 89). These bands can be straightforwardly assigned to spin-allowed and, respectively, spin-forbidden MLCT excited states, characteristic of the Os(II) polypyridine complexes.[90] In a rigid methanol/dichloromethane (1:1 v/v) matrix at 77 K, $[(bpy)_2Os(\mathbf{10})Os(bpy)_2]^{4+}$ shows a structured emission band with λ_{max} = 735 nm (Figure 89) and τ = 0.97 µs, again typical of Os(II) polypyridine complexes.[90]

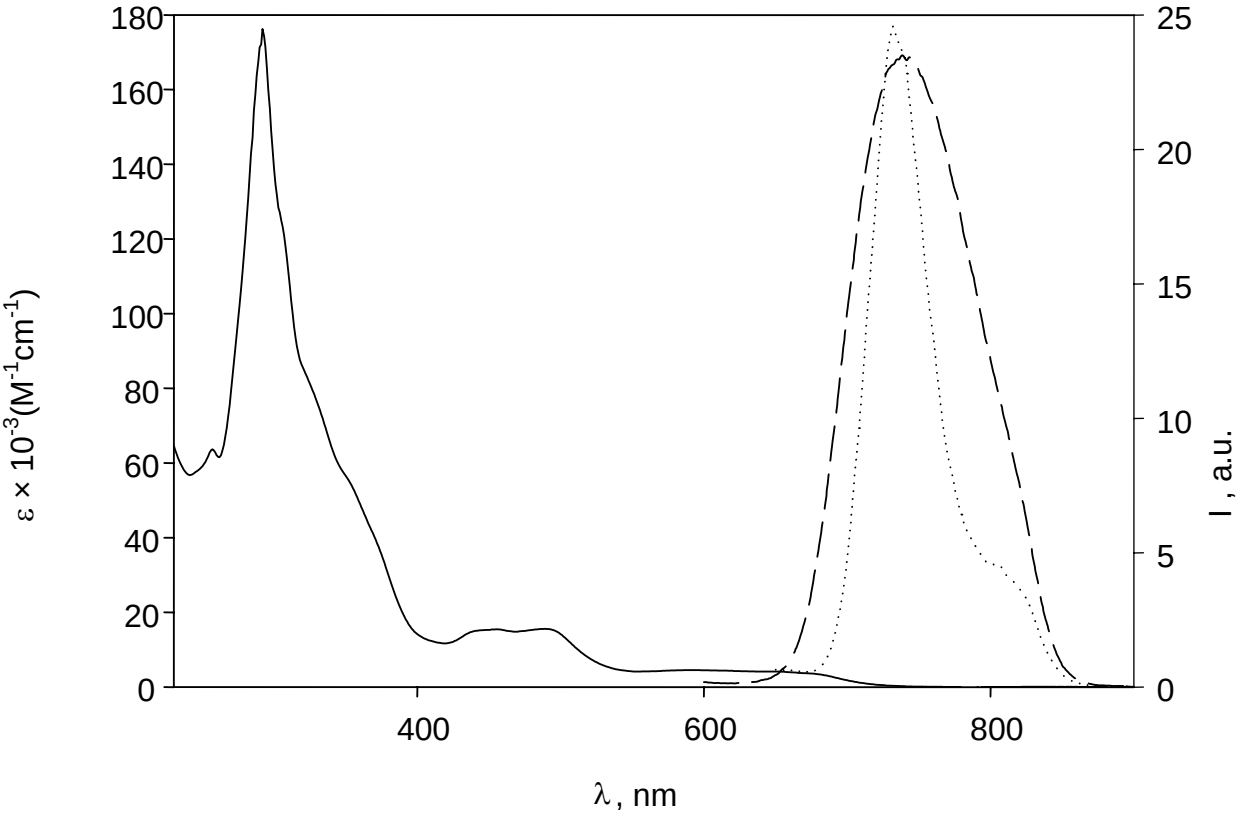

Figure 89. Absorption (dichloromethane solution; full line) and emission (dichloromethane solution at 298 K, dashed line; methanol/dichloromethane rigid matrix at 77 K, dotted line) spectra of the $[(bpy)_2Os(\mathbf{10})Os(bpy)_2]^{4+}$ complex.

4.6.4. Electrochemical properties of macrocycle 10 and its Ru, Os, and mixed Ru/Os complexes

Electrochemical properties of macrocycle 10

The electrochemical properties of compound **10** were investigated in purified tetrahydrofuran under vacuum conditions. In the accessible potential window (+1/–3 V vs SCE), compound **10** undergoes three reversible bielectronic reduction processes at –1.76, –1.94, and –2.07 V *vs* SCE, a fourth irreversible reduction process at –2.36 V *vs* SCE, and no oxidation process (Table 12). A comparison with the data obtained under the same conditions for **10**, and bpy ligand (Table 12) shows that (i) the macrocyclic ligand **10** is easier to reduce than the bpy and (ii) the two bpy units of **10** are equivalent and behave independently as indicated by the fact that they are reduced simultaneously at the same potential value.

Table 12. Electrochemical properties of macrocycle **10**, $[(bpy)_2Ru.\mathbf{10}.Ru(bpy)_2]^{4+}$, $[(bpy)_2Os.\mathbf{10}.Os(bpy)_2]^{4+}$, $[(bpy)_2Ru.\mathbf{10}.Os(bpy)_2]^{4+}$, and some model compounds.[a]

	Ligand centered reduction $E_{1/2}$ (ΔV)[b] [n][c]				Metal centered oxidation $E_{1/2}$ (ΔV)[b] [n][c]	
					Os	Ru
10 [d,e]	−2.36 [f]	−2.07 (60) [2]	−1.94 (60) [2]	−1.76 (66) [2]		
$Ru^{II}.\mathbf{10}.Ru^{II}$ [d]			−1.43 (80) [2]	−1.13 (70) [2]		+1.44 (80) [2]
$Os^{II}.\mathbf{10}.Os^{II}$ [d]			−1.35 (105) [2]	−1.06 (100) [2]	+1.03 (90) [2]	
$[Ru(bpy)_3]^{2+}$ [d]			−1.50 (90) [1]	−1.24 (70) [1]		+1.43 (78) [1]
$[Os(bpy)_3]^{2+}$ [d]			−1.35 (100) [1]	−1.06 (90) [1]	+1.03 (90) [1]	
bpy [d,e]			−2.69 [f]	−2.18 (100) [1]		
$Ru^{II}.\mathbf{10}.Os^{II}$		−1.42 (60) [1	−1.36 (60) [1	−1.09 (84) [2]	+1.01 (60) [1]	+ 1.45 (60)[1]

[a] Room temperature argon-purged dichloromethane solution, unless otherwise noted; halfwave potential values in V vs SCE; tetrabutylammonium hexafluorophosphate as supporting electrolyte, glassy carbon as working electrode. [b] Average value of the $|E_a - E_c|$ in mV. [c] Number of the exchanged electrons. [d] Data obtained from literature. [e] Purified tetrahydrofurane under vacuum conditions. [f] Irreversible process; potential value estimated by the DPV peak.

Electrochemical properties of $[(bpy)_2Ru(10)Ru(bpy)_2](PF_6)_4$

In the electrochemical experiments performed in argon-purged dichloromethane solution, $[(bpy)_2Ru(\mathbf{10})Ru(bpy)_2]^{4+}$ undergoes a reversible bielectronic oxidation at +1.44 V *vs* SCE (Figure 90, Table 12), that can be assigned to the concomitant oxidation of the two metal-centers.[48a] This result shows that the two metal centers of $[(bpy)_2Ru(\mathbf{10})Ru(bpy)_2]^{4+}$ are equivalent and do not interact with one another. The potential value at which the two Ru ions are simultaneously oxidized is very similar to that observed for the metal oxidation in $[Ru(bpy)_3]^{2+}$. On reduction, two reversible bielectronic processes are observed in the accessible potential window, which can be attributed to the reduction of the ligands (Figure 90). By comparison with the data obtained for and $[Ru(bpy)_3]^{2+}$, these processes can be easily assigned as follows: (i) the first process at –1.13 V *vs* SCE concerns the simultaneous reduction of the two bpy units of the ligand **10**, considering that such a ligand is easier to reduce than the bpy ligand; (ii) the second process at –1.43 V *vs* SCE involves two bpy ligands, one for each $Ru(bpy)_2$ moiety, that are reduced simultaneously at the same potential. This process occurs at a potential value which is (a) more negative than that of the first

reduction of $[Ru(bpy)_3]^{2+}$, because in the dinuclear complex the bpy ligand reduction is preceded by the reduction of the bpy units of ligand **10**, and (b) less negative than that of the second reduction of $[Ru(bpy)_3]^{2+}$ because of the different reducibility of bpy and ligand **10** and the greater delocalization of the charges introduced by replacing one bpy with the ligand **10**.

Electrochemical properties of $[(bpy)_2Os(10)Os(bpy)_2](PF_6)_4$

In the electrochemical experiments performed in argon-purged dichloromethane solution, $[(bpy)_2Os(\mathbf{10})Os(bpy)_2]^{4+}$ undergoes a reversible bielectronic oxidation at +1.03 V *vs* SCE (Figure 90), that can be assigned to the concomitant oxidation of the two metal-centers.[48a] As already discussed for $[(bpy)_2Ru(\mathbf{10})Ru(bpy)_2]^{4+}$, this result shows that the two Os centers are equivalent and do not interact with one another. The potential value at which the two Os ions are simultaneously oxidized is identical to that obtained for the metal oxidation in $[Os(bpy)_3]^{2+}$ (Table 12). On reduction, two reversible bielectronic processes are observed in the accessible potential window. In agreement with the above discussed dinuclear Ru-based complex, the first process at –1.06 V *vs* SCE can be assigned to the reduction of ligand **10**, while the second process at –1.35 V *vs* SCE concerns the simultaneous reduction of two bpy ligands, one for each $Os(bpy)_2$ moiety. The fact that these processes occur at the same potential values observed for $[Os(bpy)_3]^{2+}$ (Table 12) can be explained considering that the Os(II) ion is capable to delocalize the introduced charges better than the Ru(II) ion.[89]

Electrochemical properties of $[(bpy)_2Ru(10)Os(bpy)_2](PF_6)_4$

The cyclic voltammogram obtained for $[(bpy)_2Ru(\mathbf{10})Os(bpy)_2]^{4+}$ in argon-purged dichloromethane solution is displayed in Figure 91 and the potential values are shown in Table 12. The oxidation processes of the Os(II) (1.01 V *vs* SCE) and Ru(II) (1.45 V *vs* SCE) units in $[(bpy)_2Ru(\mathbf{10})Os(bpy)_2]^{4+}$ are well separated and occur almost at the same potentials as the Os(II) and Ru(II) units of the respective homodinuclear and mononuclear species, showing that there is no appreciable interaction between the two metal centers within the limits of the electrochemical technique.[91] The reduction potentials are also in line with successive independent reductions of the ligands of the two units. Comparison with the potential values obtained for the other compounds[81] allows us to assign (i) the first process at –1.09 V *vs* SCE to the simultaneous reduction of the two bpy units of the ligand **10**, which is easier to reduce than the bpy, and (ii) the second and third processes at –

1.36 and –1.42 V *vs* SCE to the reduction of a bpy ligand of the Os(II) and Ru(II) moieties, respectively.

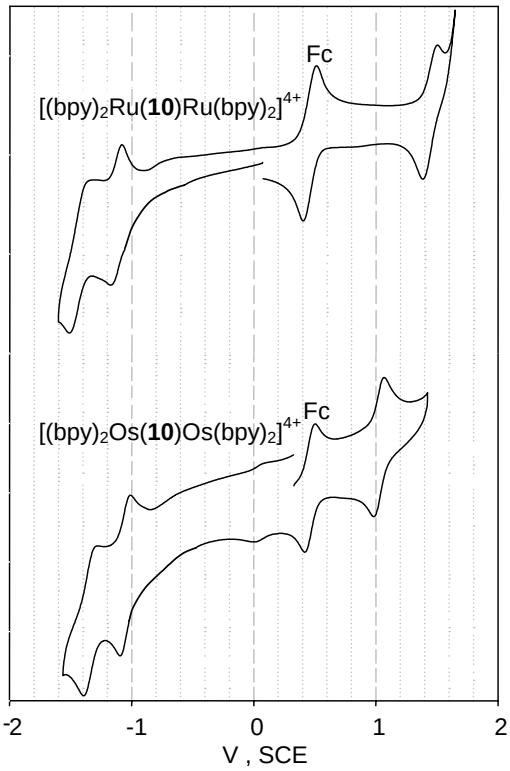

Figure 90. Cyclic voltammograms obtained for the Ru and Os complexes of macrocycle **10** (argon-purged dichloromethane; complex concentration 1×10^{-3} M; glassy carbon as working electrode, scan rate of 200 mV/s); Fc indicates the wave of the ferrocene added as internal reference.

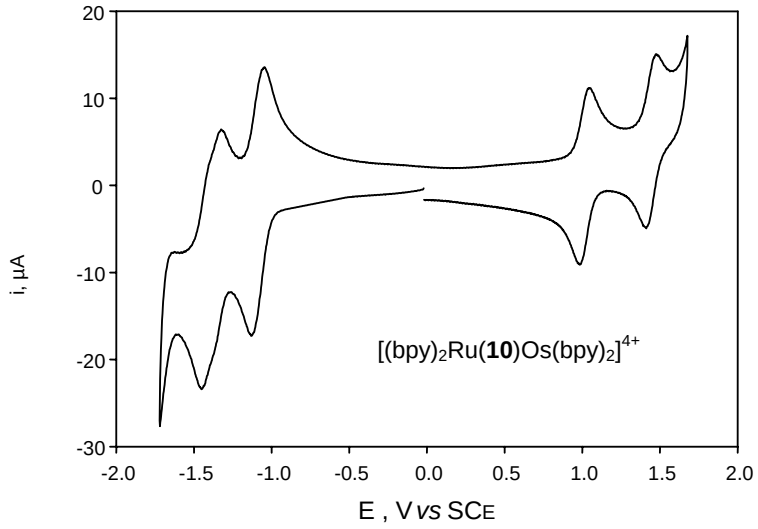

Figure 91. Cyclic voltammogram obtained for the $[(bpy)_2Ru(\mathbf{10})Os(bpy)_2]^{4+}$ complex (argon-purged dichloromethane; complex concentration 5.0×10^{-4} M; glassy carbon as working electrode, scan rate of 100 mV/s).

4.6.5. Photophysical properties of the mixed Ru/Os complex of macrocycle 10

Spectroscopic properties of $[(bpy)_2Ru(10)Os(bpy)_2]^{4+}$

The absorption spectrum of $[(bpy)_2Ru(\mathbf{10})Os(bpy)_2]^{4+}$ in acetonitrile solution is displayed in Figure 92 where the spectra of the homodinuclear $Ru^{II}.\mathbf{10}.Ru^{II}$ and $Os^{II}.\mathbf{10}.Os^{II}$ compounds are also shown for comparison purposes (the complexes were renamed $M^{II}.\mathbf{10}.M^{II}$).

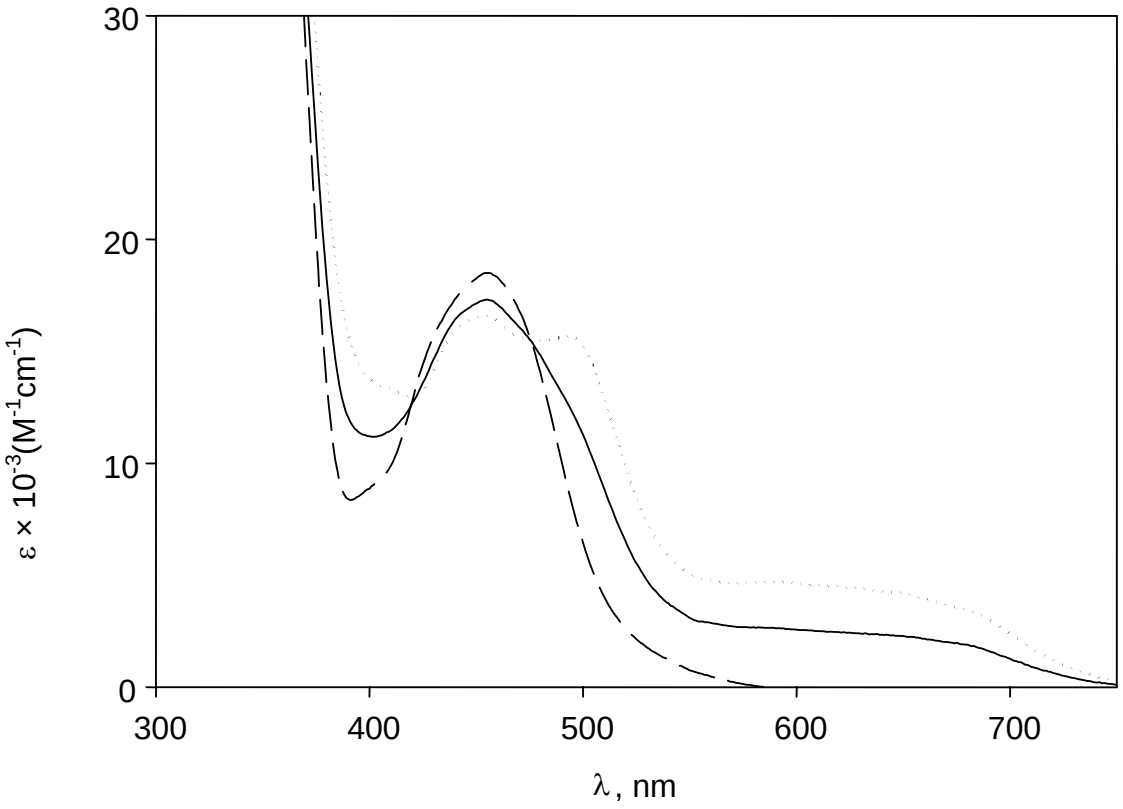

Figure 92. Absorption spectra of $Ru^{II}.\mathbf{10}.Os^{II}$ (full line), $Ru^{II}.\mathbf{10}.Ru^{II}$ (dashed line), and $Os^{II}.\mathbf{10}.Os^{II}$ (dotted line) (acetonitrile solution at 298 K).

It is well known that the bands in the visible spectral region are due to metal-to-ligand charge-transfer (MLCT) transitions.[48a], [90] It can be noticed that for the Os-based chromophoric units, even the formally forbidden triplet-triplet transitions (550-750 nm region) display a considerable intensity because of the heavy atom effect. The absorption spectrum of $Ru^{II}.\mathbf{10}.Os^{II}$ is equal to that of a 1:1 mixture of

the homodinuclear Ru^{II}.**10**.Ru^{II} and Os^{II}.**10**.Os^{II} parent compounds. This, however, is not the case for luminescence (Figure 93).

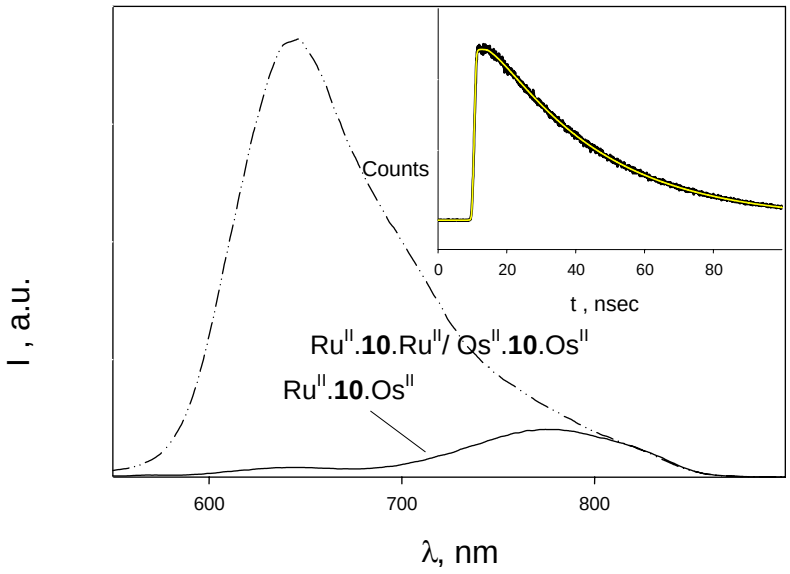

Figure 93. Comparison of the luminescence spectra (air-equilibrated acetonitrile solution at 298 K, λ_{exc} = 475 nm) of Ru^{II}.**10**.Os^{II} complex (full line) and of a 1:1 mixture of the Ru^{II}.**10**.Ru^{II} and Os^{II}.**10**.Os^{II} compounds (dashed and dotted line). Inset shows the rise and the decay of the Os-based excited state (λ_{exc} = 406 nm; λ_{em} = 780 nm).

Upon excitation in the isosbestic point at 475 nm, the luminescence spectrum of a 1:1 mixture of the Ru^{II}.**10**.Ru^{II} and Os^{II}.**10**.Os^{II} compounds is dominated by the much stronger (Table 13) Ru-type emission with maximum at 645 nm, whereas in the heterodinuclear Ru^{II}.**10**.Os^{II} compound this band is almost completely quenched and the Os-type band with maximum at 780 nm predominates.

Table 13. Luminescence properties

	298 K[a]						77 K[b]			
	Ru			Os			Ru		Os	
	λ_{max} , nm	τ , ns	I_{rel}	λ_{max} , nm	τ , ns	I_{rel}	λ_{max} , nm	τ , μs	λ_{max} , nm	τ , μs
Ru^{II}.**10.**Os^{II}	645	4.9 (78%) 45 (22%)	3	780	31[d]	97			735	1.1[e]
Ru^{II}.**10**.Ru^{II}	645	285	100	-	-	-	600	5.14	-	-
Os^{II}.**10**.Os^{II}	-	-	-	780	31	100	-	-	735	1.0
$[Ru(bpy)_3]^{2+}$	615	170	25[f]	-	-	-	580	2.0	-	-
$[Os(bpy)_3]^{2+}$	-	-	-	740	49	91[g]	-	-	710	0.8

[a] Air-equilibrated acetonitrile. [b] Butyronitrile rigid matrix. [c] Excitation was performed at 475 nm, which is an isosbestic point between the Ru-based and Os-based units on equimolar solutions; for comparison purposes, the luminescence intensities of Ru^{II}.**10**.Ru^{II} at 645 nm and Os^{II}.**10**.Os^{II} at 780 nm were taken as 100. [d] To be compared with the risetime of the Os-based emission (7.3 ns). [e] To be compared with the risetime of the Os-based emission (50 ns). [f] The luminescence quantum yield under these conditions is 0.016. [g] The luminescence quantum yield under these conditions is 3.5×10^{-3}.

Intercomponent energy transfer in Ru^{II}.10.Os^{II}.

The results obtained showed that 97% of the luminescence intensity of the Ru-based component is quenched by the presence of the Os-based component. The quenching of the Ru-based excited state takes place by energy transfer to the Os-based unit. Since the lifetime of the (unquenched) Ru-based excited state is 285 ns and the concentration of Ru^{II}.**10**.Os^{II} was 5.0×10^{-5} M, *intermolecular* quenching can be ruled out and it was conclude that in this compound the quenching by energy transfer occurs *intramolecularly* (Figure 94).

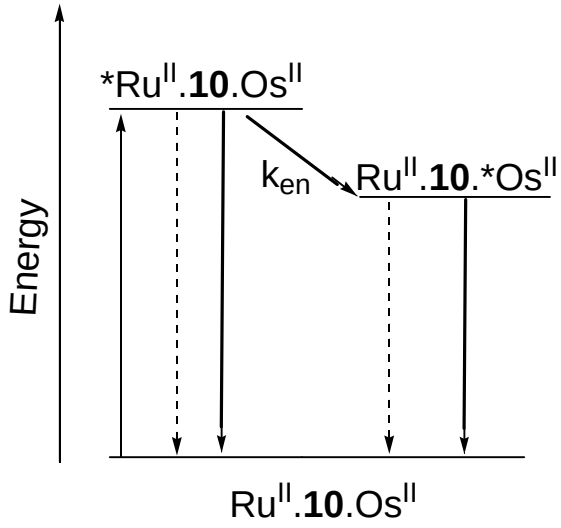

Figure 94. Energy-level diagram showing the photoinduced energy-transfer processes that occur in Ru^{II}.**10**.Os^{II} complex. Key: full line, excitation; dashed line, luminescence; wavy line, radiationless decay.

As expected for an energy-transfer process, the decay of the Ru-based excited state is accompanied by the rise of the Os-based excited state (Figure 93, inset). Since selective excitation of the Ru-based chromophoric unit cannot be obtained (λ_{exc} = 406 nm), a substantial fraction of Os-based excited states is already present when the Os-based excited state originating from energy transfer begins to accumulate. This is also the reason why it is difficult to distinguish two different components in the rise of the Os-based emission.

The rate constant for the energy-transfer processes can be calculated from the following relation:

$$k_{en} = 1/\tau - 1/\tau^{\circ} \qquad (1)$$

where τ and τ° are the luminescence lifetimes of the Ru-based component in Ru^{II}.**1**.Os^{II} and in the Ru^{II}.**1**.Ru^{II} model compound, respectively. From the lifetimes values shown in Table 13, rate constants k_{en} 2.0×10^{8} and 2.2×10^{7} s^{-1} were obtained at 298 K.

Spectroscopic properties of the mixed-valence Ru^{II}.1.Os^{III} compound.

Titration of a 2.2×l0^{-5} M Ru^{II}.**1**.Os^{II} acetonitrile solution by an acetonitrile solution of Ce(IV) caused strong changes in the absorption spectrum, with isosbestic points at 400 and 750 nm (Figure 95).

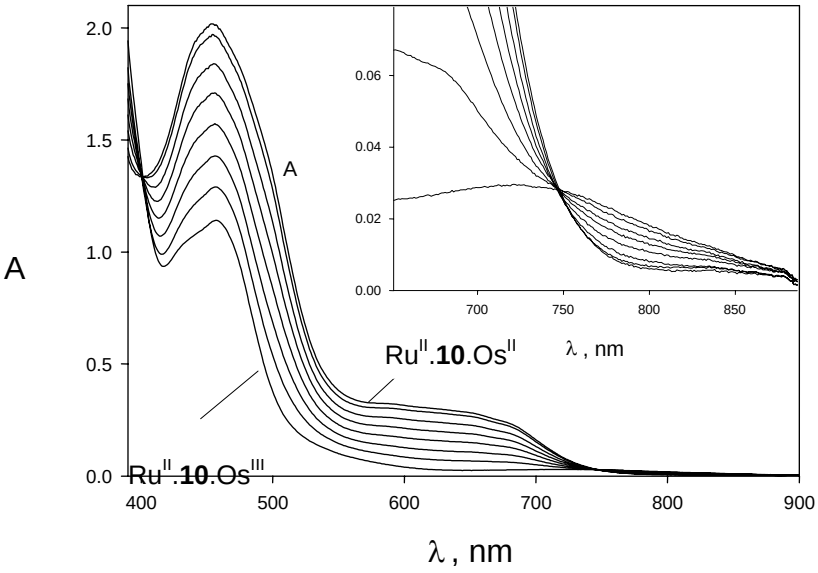

Figure 95. Absorption spectral changes observed during the titration of Ru^{II}.**10**.Os^{II} with Ce(IV) in acetonitrile solution (optical path = 5 cm). Inset shows the growth of the intervalence band during the titration.

After addition of one equivalent of oxidant, no further change was observed. The linear decrease in intensity of the MLCT absorption bands in the spectral region between 400 and 700 nm indicates that oxidation concerns only the Os-based unit.[92] It can be noticed (Figure 95, inset) that such a decrease is accompanied by the appearance of a relatively weak, broad band with maximum at 720 nm (ε_{max} = 250 M^{-1} cm^{-1}). This band cannot be assigned to the Os(III) unit generated by oxidation, since the lowest energy band of $[Os(bpy)_3]^{3+}$ (a doublet-doublet ligand-to-metal charge-transfer band) shows its maximum at 563 nm (ε_{max} =585 M^{-1} cm^{-1}).[93] The rising band can thus be assigned to an “intervalence” Ru(II) → Os(III) transition in the generated Ru^{II}.**10**.Os^{III} species. An intervalence transfer band was seldom observed[94] in previously investigated mixed valence Ru(II)-Os(III) polypyridine compounds.[95], [96], [97], [98], [99], [100]

Oxidation of the Ru^{II}.**10**.Os^{II} solution causes changes also in the emission spectrum. As we have seen above, in Ru^{II}.**10**.Os^{II} the Ru(II)-based emission is strongly, but not completely quenched by energy transfer to the Os(II)-based one (Figure 93). After addition of one equivalent of oxidant, the Os(II)-based emission band (λ_{max} = 780 nm) can no longer be observed, showing that the Os(II) unit has been quantitatively oxidized. The disappearance of the Os(II) "quenching" unit, however, does not cause a complete recovery of the of Ru(II)-based band (λ_{max} = 645 nm), but only a slight increase (7%) in intensity (Figure 96). In other words, the Ru(II)-based band is slightly less quenched in Ru^{II}.**10**.Os^{III} compared with Ru^{II}.**10**.Os^{II}.

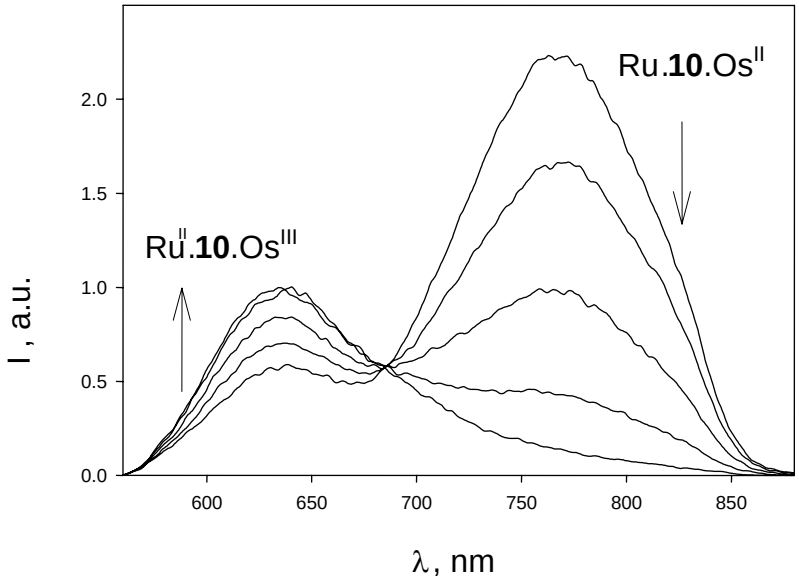

Figure 96. Normalized absorption decrease at 700 nm (full circles) and corresponding increase at 800 nm (full triangles) observed during the titration of Ru^{II}.**10**.Os^{II} with Ce(IV).

Intercomponent electron transfer in Ru^{II}.10.Os^{III}

In Ru^{II}.**10**.Os^{III} the Ru(II)-based emission is strongly quenched by the Os(III)-based one. The energy-level diagram schematized in Figure 97 shows that, in principle, the quenching of the Ru(II)-based excited state can takes place (i) by intercomponent electron transfer via direct formation of the Ru^{III}.**10**.Os^{II} excited state, which is that obtained by excitation in the intervalence transfer band, or (ii)

by intercomponent energy transfer to form the Ru^{II}.**10**.*Os^{III} species that then relaxes to the ground state via the Ru^{III}.**10**.Os^{II} intervalence transfer excited state.

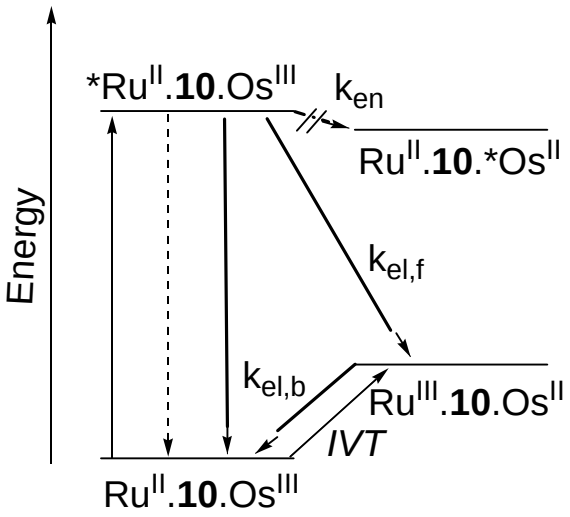

Figure 97. Energy-level diagram showing the photoinduced electron-transfer processes that occur in Ru^{II}.**10**.Os^{III} complex. Key: full line, excitation; dashed line, luminescence; wavy line, radiationless decay. The process labelled *IVT* represents the excitation in the intervalence transfer band.

With the help of laser flash photolysis experiments it was conclude that the quenching of the Ru(II)-based emission takes place by electron transfer with direct formation of the intervalence transfer excited state Ru^{III}.**10**.Os^{II}.

Flash photolysis experiments have also allowed to measure the rate of the back electron-transfer process, Ru^{III}.**1**.$Os^{II} \rightarrow Ru^{II}$.**1**.$Os^{III}$ (Figure 97), ($k_{el,b}$ 9.1×10^{7} and 1.2×10^{7} s^{-1}, Table 14).

The kinetics of three processes were investigated, namely

*Ru^{II}.**10**.$Os^{II} \rightarrow Ru^{II}$.**10**.*$Os^{II}$	energy transfer
*Ru^{II}.**10**.$Os^{III} \rightarrow Ru^{III}$.**10**.$Os^{II}$	forward electron transfer
Ru^{III}.**10**.$Os^{II} \rightarrow Ru^{II}$.**10**.$Os^{III}$	back electron transfer

For each process two distinct rate constants were found. This result indicates that each dinuclear complex exists as a mixture of two different conformers (or family of conformers).

Table 14. Experimental rate constants (air-equilibrated acetonitrile solution at 298 K) and related parameters.

	k, s^{-1}	ΔG°, eV	λ_i, eV	λ_o, eV	$exp(-\Delta G^{\neq}/RT)$	ν, s^{-1}	*H*, cm^{-1}
Energy transfer							
$^*Ru^{II}$**.10.**$Os^{II} \rightarrow Ru^{II}$**.10.**$^*Os^{II}$	2.0×10^8 2.2×10^7	–0.33	0.2	0	+0.44	4.5×10^8 5.0×10^7	0.9 0.3
Electron transfer							
$^*Ru^{II}$**.10.**$Os^{III} \rightarrow Ru^{III}$**.10.**$Os^{II}$	1.6×10^8 2.7×10^7	–1.48	0.1	1.3	+0.95	1.7×10^8 2.8×10^7	0.9 0.4
Ru^{III}**.10.**$Os^{II} \rightarrow Ru^{II}$**.10.**$Os^{III}$	9.1×10^7 1.2×10^7	–0.44	0	1.3	+0.004	2.3×10^{10} 3.2×10^9	10 4

Different conformers can indeed be expected because steric hindrance between hydrogen atoms of pyridine and phenyl rings in the bis-chelating ligand **10** forces the binuclear complexes to assume a *cis* or *trans* structure. In the *cis* structure the two metal ions lie on the same side of the plane defined by the shape-persistent macrocycle **10** and the metal-metal distance is estimated to be 1.5 nm from a space filling model, whereas for the *trans* conformer the two metal ions lie on opposite sides of the plane and their distance is about 1.7 nm. The through-bond distance, of course, is the same (ca. 2.7 nm) for both structures, but this does not mean that the through bond electronic coupling has to be the same in the two conformers. The two different rates obtained for each of the investigated processes can thus be assigned to the different conformers, but it is not easy to establish which structure exhibits the larger electronic coupling. If, as it seems possible, the energy-transfer process takes place by a through space Förster mechanism, the faster energy-transfer process should be that occurring in the *cis*-like conformer.